Computer Animation and Virtual Worlds

WILEY

RESEARCH ARTICLE OPEN ACCESS

A 3D Visual Tool for Analyzing Changes in Hair Volume and Length Caused by Medications

Jong-Hyun Kim[1] | Jung Lee[2] | Seungbin Kwon[3] | Minji Jo[3] | Yunjin Hwang[3] | In-Sook An[3]

[1]College of Software and Convergence (Department of Design Technology), Inha University, Incheon, South Korea | [2]Department of Computer Engineering, Hanbat National University, Daejeon, South Korea | [3]Korea Institute of Dermatological Sciences, Seoul, Republic of Korea

Correspondence: In-Sook An (research@skinresearch.or.kr)

Received: 13 February 2025 | **Revised:** 22 April 2025 | **Accepted:** 11 July 2025

Funding: This work was supported by the research fund of the Hanbat National University in 2023, the Inha University Research Grant, the Institute of Information & Communications Technology Planning & Evaluation (IITP) grant funded by the Korea Government (MSIT) (No. RS-2022-00155915, Artificial Intelligence Convergence Innovation Human Resources Development (Inha University)).

Keywords: 3D visual tool | hair modeling | hair volume | hairstyle | physically-based simulation

ABSTRACT

This paper proposes a 3D visual tool based on physically-based simulation to verify and analyze changes in the volume and length of hair after treatment with cosmetics or other chemicals. Unlike fur and hair simulations in virtual environments, real hair undergoes various chemical treatments not only to enhance hair quality but also to increase hair density. Such treatments are important as they lead to hairstyling, which significantly affects a person's impression. We propose a novel visual tool that visualizes and analyzes changes in the length and volume of original strands before and after chemical treatment based on physically-based hair simulation. The results are applied to various scenarios, including back hair volume, root hair volume, side hair volume, crown hair volume, and hair sagging, to evaluate its effectiveness.

1 | Introduction

Key elements for a detailed representation of digital humans in virtual environments include hair modeling, rendering, and simulation [1–3]. Hairstyles and fur play a crucial role in representing characters in virtual environments, but also in completing a person's styling in the real world. Hair is one of the most dynamically changing features of the human body [4]. However, when hair strands lose length and volume due to damage, many people use various chemicals, including cosmetics, to compensate [5]. Most previous studies have been conducted in 2D environments; this study proposes a 3D visual tool for analyzing strand volume and length before and after chemical treatment in a 3D environment.

When performing human application tests on scalp cosmetics for hair curling durability, root volume, crown volume, overall hair volume, side hair volume, and back hair volume, digital cameras are commonly used. Hair photographs are taken before and after application of the product under consistent conditions such as angle, distance, and lighting. Image analysis programs (e.g., ImageJ or Image Pro 10) are then used to analyze hair length, height, area, width, and angle, and the data are extracted to evaluate improvements. However, since the hair images used are 2D, it is difficult to fully assess the overall hair structure. By inputting the numerical data obtained from actual hair tests to reconstruct the 3D geometry of hair before and after product use, it becomes possible to predict the shape of the hair after cosmetic application in three dimensions rather than on a 2D plane. This approach

All authors contributed equally to this article.

provides users with three-dimensional information, making it easier to understand the results of tests conducted before and after product use.

In this study, the 3D space is represented as a hexahedron, allowing accurate proportional verification of hair changes before and after testing. This allows for three-dimensional analysis from various angles and perspectives to match the desired efficacy and effects of hair/scalp cosmetics or hair beauty devices. From the perspective of product manufacturers, this approach enhances realism and immersion for consumers, delivering visually impactful product results. For consumers, it offers the advantage of previewing the efficacy of hair products in three dimensions without the need to try them directly. Furthermore, since the overall appearance and shape of hair, rather than its individual parts, significantly influence a person's impression, three-dimensional visualization is essential. Although 2D images only provide a view from one side, this study enables the extraction of 3D hair images from multiple angles, allowing users to observe various aspects of hair changes. This dynamic and realistic 3D imagery can capture consumers' attention and interest in marketing, making it a powerful tool to convey product results effectively.

2 | Related Work

This section examines various techniques for representing hair in virtual environments.

2.1 | Hair Capture

There have been numerous studies on reconstructing hair from multiple images. Paris et al. introduced a method to estimate the 3D orientation of hair based on highlights observed under various lighting conditions and synthesized the full strands accordingly [6]. Wei et al. proposed a technique to compute the 3D orientation of hair from multi-view images by optimizing orientation consistency across different views [7]. Paris et al. also developed a system to accurately acquire the positions of hair strands using projected light beams and a diffusion scheme to interpolate the orientation field [8]. Jakob et al. demonstrated the potential to identify focused hair strands in multiple views using a moving macro lens with shallow depth-of-field [9].

Chai et al. proposed a method for generating 3D strands from a single image by considering inter-strand occlusions [10]. This system was extended to generate hair animation from a single video input, but was limited to relatively simple hairstyles [11]. Beeler et al. presented a multi-view stereo system for reconstructing short facial hair using strand-level matching [12]. Their approach included a refinement step to improve strand connections and eliminate outliers. Herrera et al. proposed a hair capture system using a thermal imaging device, achieving impressive results, although it was less suitable for capturing hair far from the head [13].

Luo et al. introduced a method for reconstructing an approximated surface-to-hair volume based on a multi-view orientation field [14, 15]. They also proposed a method for reconstructing hair from point-cloud data [16]. Hu et al. suggested a method for hair reconstruction using a database of simulated hair strand examples [17].

In another study, Hu et al. proposed a framework that synthesizes new hair models by comparing user strokes with a hairstyle database [18]. Chai et al. introduced a method for generating high-quality hair models for 3D printing applications [19]. Chai et al. also proposed a method for creating hair models from a single photo, but the hair shape at the back of the head is often handled with strong assumptions, leading to potentially inaccurate results [20]. Zhang et al. used four-sided hair images to infer hair modeling [21]. This study required a hair model database that could individually match and combine images from each side to generate an approximate hair model.

Recently, Sklyarova et al. proposed a high-quality 3D hair reconstruction method applicable in real-world environments, restoring human hair at the strand level through a two-stage process [22]. The first stage, Coarse Reconstruction, infers rough hair shape and orientation information from input data such as videos or multi-camera setups. The second stage, Fine Strand-based Reconstruction, uses the output from the first stage along with a learned hair prior to compute a high-resolution 3D model that includes individual hair strands. While the method enables robust reconstruction from both single images and multi-view inputs, it has limitations in representing curly hair. Despite the use of curvature loss, it struggles to handle complexly twisted hair structures. Moreover, the computational cost is significant, requiring approximately three days of processing on an RTX 4090 GPU.

We et al. proposed a method for high-quality 3D hair reconstruction from a single-camera video input [23]. Their approach generates results without requiring specific lighting, controlled environments, or specialized equipment, and it can capture fine external details of real images even without data priors. Compared to existing methods such as Neural Haircut, it achieves more than 10× faster sequential performance, improving its practicality [22]. It enables strand-level reconstruction using only a monocular camera and supports various hairstyles, including curly hair. However, the internal structure still relies on data priors, so additional data is needed to ensure broader generalizability.

Zhou et al. proposed a novel pipeline for high-precision strand reconstruction using multi-view images without relying on external data priors [24]. Based on a NeRF architecture, their method infers a high-resolution implicit volume representing 3D orientation information, overcoming the common issue of over-smoothing and preserving fine directional details. It enables accurate reconstruction of various hairstyles without depending on specific datasets and achieves more detailed 3D orientation field rendering than previous approaches. However, it requires substantial computational resources and processing time.

2.2 | Hair Simulation

Real-time hair simulation techniques based on Position-Based Dynamics (PBD) have been extensively studied in recent

years [25, 26]. PBD has been applied to simulate various fluid-based materials, including cloth, soft bodies, liquids, smoke, sand, and hair [25, 27–29]. Han and Harada proposed a real-time hair simulation method using local and global shape constraints [30]. Kim et al. introduced a long-range attachment constraint to enforce inextensibility in hair simulations using PBD [31]. Umetani et al. simulated curly hair using PBD by applying constraints to the Darboux vector [32].

In the broader category of hair simulation, to reduce computational complexity similar to fluid continuum, hair motion is often represented as an aggregated medium [33]. A technique more suitable for generating a strand database is strand-level simulation based on strand dynamics. In the past, many mechanical strand models have been studied. Selle et al. proposed a simple mass-spring model for efficient and robust hair simulation [34]. Bergou et al. introduced discrete elastic rods, an efficient simulation framework based on explicit centerline representation using reduced coordinates [35]. Bertails et al. utilized the Cosserat rod model with piecewise helical discretization, enabling efficient hair simulation with a very small number of elements [36].

2.3 | Implcit Nueral Representation

Recently, studies have extensively explored representing 3D geometry in an implicit way due to its simplicity and efficiency [37–40]. For example, Park et al. mapped 3D coordinates to signed distance functions, representing 3D shapes using an MLP (Multilayer Perceptron) [39]. Mescheder et al. proposed a novel network that represents continuous surfaces as 3D occupancy fields, generating high-quality results at infinite resolution [41]. However, these methods rely on global latent codes to represent entire 3D shapes, limiting them to simple shapes and lacking robustness in their algorithms.

To address these limitations, several studies have focused on combining local features to represent 3D shapes instead of directly encoding the entire shape into a global latent code [42–45]. Saito et al.'s PIFu (Pixel-aligned Implicit Function) learns per-pixel implicit representations from global context and pixel-aligned features, enabling high-fidelity reconstruction while preserving local details [45]. Similarly, Jiang et al. proposed a local implicit grid representation for arbitrary objects or scenes, significantly improving the generalizability of the network [46].

As mentioned earlier, most approaches focus on reconstructing or simulating virtual hair from a few images, but studies addressing the characteristics of real hair are relatively scarce. This study proposes a method to quickly visualize and analyze changes in hair volume and length caused by chemical treatments using a 3D visual tool.

3 | Proposed Framework

In this section, we model 3D strands to measure and visualize changes caused by chemical treatments, considering the following aspects: (1) strand sagging, (2) changes in root volume, (3) changes in crown volume, (4) changes in back volume, and (5) changes in side volume (see Figure 1).

3.1 | Sagging of Hair Before and After Chemical Treatment

In this section, we propose a method to visualize changes in hair sagging before and after chemical treatment in 3D. Specifically, we present a strand modeling technique that enables rapid visualization for straight and curly hair. The input data includes the actual measured length and texture, and the real-time visualization is ultimately performed in the form shown in Figure 2.

The input length data consists of the actual measured values. However, for 3D visualization, the length ratio σ_d was used and the actual length was not included in this process (see Equation (1)).

$$\sigma_d = \frac{d^{after}}{d^{before}} \tag{1}$$

where $d^{before,after}$ represents the actual measured length of the strand. Since chemical treatment tends to shorten strand length, σ_d was designed as described above in this study, but it can be flexibly modified for the opposite case as well. For straight hair, the weights for curly hair were adjusted to ensure a natural representation of straight hair.

The position of each particle constituting straight hair, $p_i^{straight}$, is calculated as shown in Equation (2).

$$p_i^{straight} = lerp\left(p^{tip}, p^{root}, w\right) \tag{2}$$

where $lerp$ represents linear interpolation, w is the weight, and $p^{root,tip}$ are the positions of the root and tip particles constituting the strand. The weight w used in $lerp$ is calculated using the particle index of the strand as $w = \frac{i}{size-1}$, where i is the particle index within the strand, increasing progressively from the root to

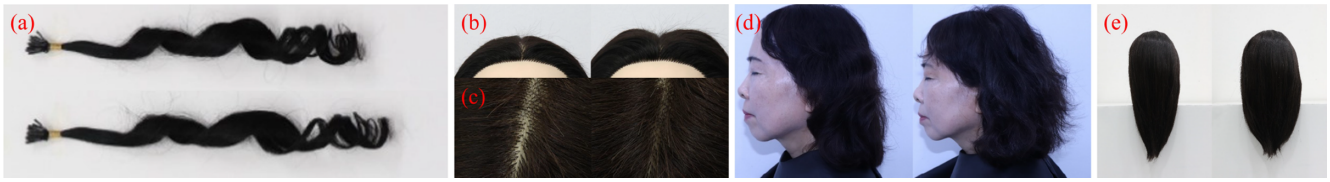

FIGURE 1 | Changes in actual strands observed from various aspects after chemical treatment. (a) Strand sagging, (b) root volume of hair, (c) crown volume of hair, (d) side volume of hair, and (e) back volume of hair.

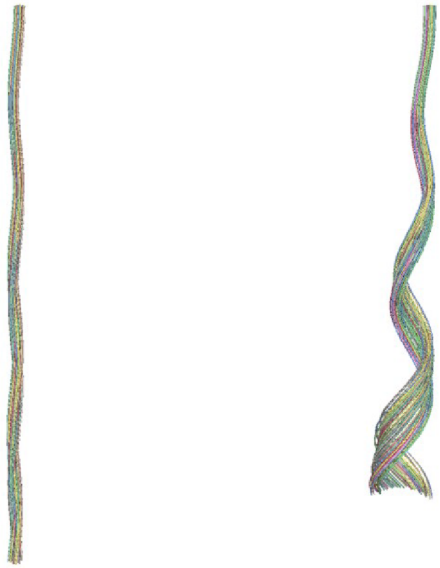

(a) Before : 24.4cm (b) After : 21.12cm

FIGURE 2 | Visualization results of hair sagging before and after chemical treatment. The reference image for (a) is shown at the *bottom* of Figure 1a, while the reference image for (b) appears at the *top* of Figure 1a.

the tip. $Size$ is the total number of particles in the strand. p^{root} is the user-defined position, and the tip position p^{tip} is calculated as shown in Equation (3).

$$p^{tip} = \left(\mathbf{y} \cdot d^{strand}\right) + p^{root} \tag{3}$$

where $\mathbf{y}$ is the up vector, set to $(0, -1, 0)$ in this study, and d^{strand} represents the total length of the strand. Since curly hair has a cylindrical volume, the position of p^{root} was adjusted, with $p^{root}.x$ set as an offset by r where r is the radius parameter for representing curly hair, which can be modified by the user.

Calculating the particle positions for curly hair is slightly more complex. To model a spiral strand, the values for the angle (α) and step (β) must be determined, where β is set to the same value as w, and α is calculated as shown in Equation (4).

$$\alpha = \frac{d^{strand}}{(size - 1)r} + \varphi \tag{4}$$

where φ is a jitter added to model the spiral strand more naturally. In this study, the min/max range for φ was set and applied as follows: $\varphi \in rand([-0.5, 0.03])$.

The curl position for representing a spiral strand is calculated as a combination of cosine and sine functions, as shown in Equation (5).

$$p_i^{curl} = \left((\mathbf{x}cos(i \cdot \alpha) + \mathbf{z}sin(i \cdot \alpha) - \mathbf{x})r + p^{root}\right) + \mathbf{y}i\beta \tag{5}$$

where $\mathbf{x}$ and $\mathbf{z}$ are the basis vectors in the space where the spiral strand is to be represented, set as $(1, 0, 0)$ and $(0, 0, 1)$, respectively.

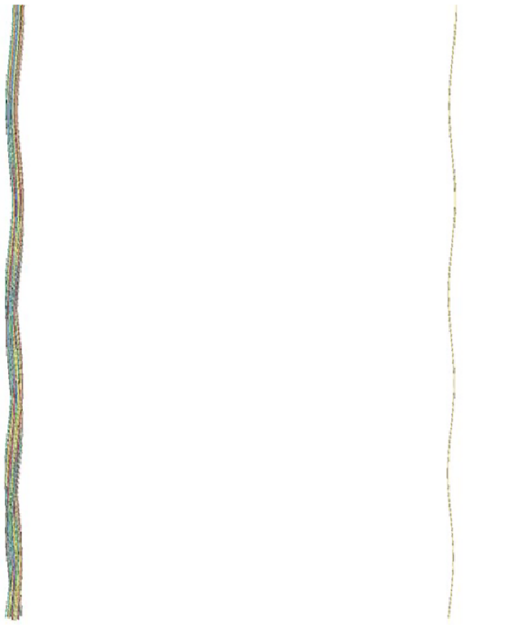

(a) $size$: 100 (b) $size$: 1

FIGURE 3 | The strand form of the straight hair equivalent.

The final positions of the hair particles are calculated by interpolating the previously computed positions for straight and curly hair, as shown in Equation (6).

$$p_i^{strand} = lerp\left(p_i^{straight}, p_i^{curl}, w\right) \tag{6}$$

In this study, to apply the changes in length after chemical treatment, the pre-treatment strand length was set as follows: $(d^{strand} = 1)$, and the post-treatment strand length was set as $(d^{strand} = 1 - \sigma_d)$. Furthermore, before treatment, the value of w used in Equation (6) was set to 0.1. Figure 3 visualizes the pre-treatment state of straight hair using our method. To achieve a more natural strand shape rather than maintaining a strictly linear form, curly strands were appropriately interpolated. As shown in Figure 3, the method successfully represented a natural hairstyle regardless of the number of strands. Figure 4 shows the results of the representation of strands shortened to curly forms after chemical treatment. Various parameters, such as strand length, angle, and count, were used to depict curly hairs. The interpolation of straight and curly strands effectively conveyed a natural curly-strand appearance.

3.2 | Changes in Root Volume Before and After Chemical Treatment

In this section, we propose a method for visualizing changes in root volume before and after chemical treatment in 3D (see Figure 5). A key aspect is ensuring a seamless and natural transition between areas where volume increases and those that remain unchanged. In addition, we present a modeling technique for the rapid visualization of strands.

FIGURE 4 | The strand form of the curly hair equivalent.

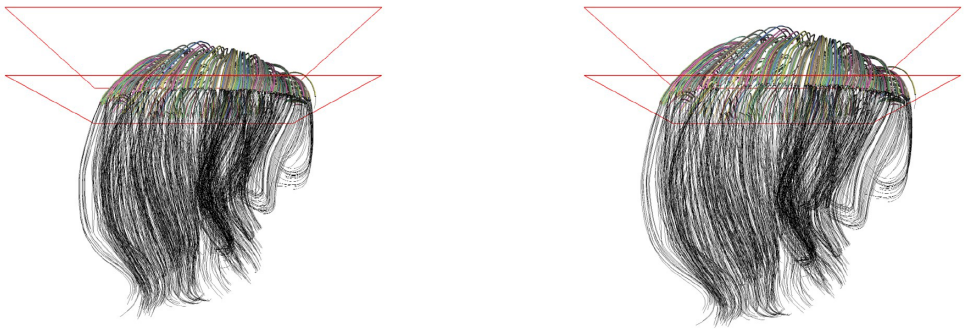

(a) Before : 2.32cm (b) After : 3.41cm

FIGURE 5 | Visualization of the root volume area before and after chemical treatment. The reference image for (a) is shown at the *left* of Figure 1b, while the reference image for (b) appears at the *right* of Figure 1b.

In this study, we defined root volume as the height from the forehead to the top of the head, considering it a key factor before and after chemical treatment (the rectangular red area in Figure 5). A hairstyle that clearly exhibits root volume was selected for modeling (see Equation 7).

$$p_i^{strand} = p^{\oplus} + \nabla p \sigma_d W\left(p_i - p^{\oplus}, h\right) \tag{7}$$

where σ_d is the weight used for hair length changes before and after chemical treatment, and $p^{\oplus}$ represents the center of mass in the root volume area (see the rectangular red area in Figure 5). The gradient ∇p is calculated as follows: $\nabla p = p_i - p^{\oplus}$. Additionally, W is an isotropic kernel, which is computed as shown in Equation (8) (see Figure 6).

$$W(\mathbf{r}, h) = \begin{cases} 1 - \frac{\|\mathbf{r}\|^2}{h^2} & 0 \le \|\mathbf{r}\| \le h \\ 0 & \text{otherwise} \end{cases} \tag{8}$$

where h is the radius of support. Due to the kernel W, the deformation of the root volume is strongly emphasized in the targeted areas, while strands outside the range of h remain unaffected. This ensures a seamless and natural transition in the deformation.

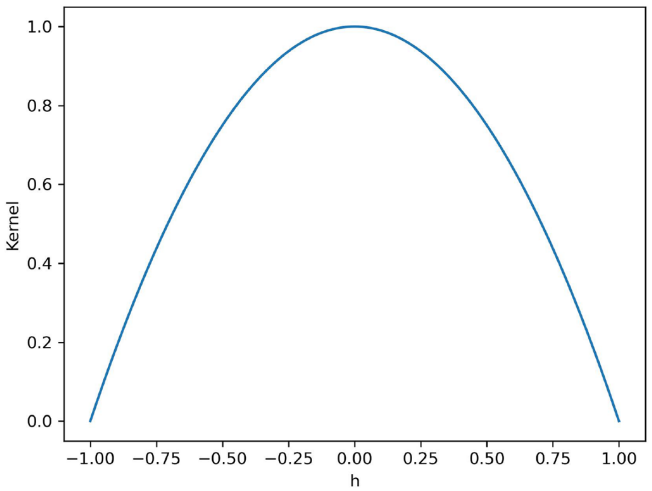

FIGURE 6 | The shape of kernel W inside the support radius $h = 1$.

3.3 | Changes in Crown Volume Before and After Chemical Treatment

In this section, we propose a method for visualizing crown volume before and after chemical treatment in 3D. The key aspect of this process is to ensure a seamless transition between areas

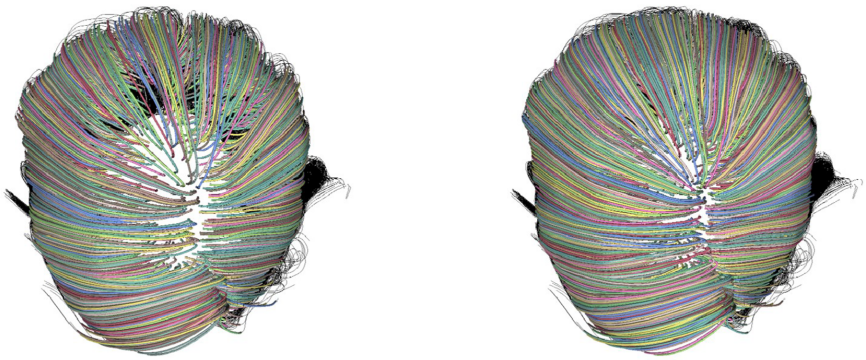

(a) Before : 7.93cm (b) After : 4.14cm

FIGURE 7 | Visualization of the crown volume area before and after chemical treatment. The reference image for (a) is shown at the *left* of Figure 1c, while the reference image for (b) appears at the *right* of Figure 1c.

where volume increases and those that remain unchanged. To achieve this, we present a strand modeling technique for rapid visualization (see Figure 7).

While root volume was measured by comparing the height from the forehead to the hair, crown volume is evaluated by comparing hair density before and after chemical treatment, as shown in Figure 7. Since hair loss is typically more noticeable along the parting and crown areas, this study adopts the following method to represent hair thinning. In this scene, a hairstyle that effectively highlights hair density is selected for modeling (see Equation (9)).

$$\Upsilon\left(p^s_{root}, r\right) = \begin{cases} \Gamma_{inside}.add\left(p^s_{root}\right) & \chi\left(p^s_{root}, r\right) < 0 \\ \Gamma_{outside}.add\left(p^s_{root}\right) & \text{otherwise} \end{cases} \tag{9}$$

where p^s_{root} represents the root particle position of each strand, and r is the range used in Γ, which is set to 0.2 in this study. χ follows the standard sphere equation, where the radius is r and the center position is p_{cp}. The value p_{cp} corresponds to the center of mass of the hair model, and $\mathbf{y}$ is set to the maximum y-position of the hair particles. Consequently, Υ is a function that classifies root particles as either inside or outside the defined range. The classified results are selectively stored in each buffer Γ, and to represent hair loss through random sampling, Γ_{inside} is shuffled using the $shuffle$ function.

Next, based on randomly shuffled root particles, hair loss strands are selected. The key aspect of this process is to determine how to represent hair loss using the parameter τ, which represents the number of lost strands: $\tau = \sigma_d \kappa \left\| \Gamma_{inside} \right\|$ where κ is a user-defined weight, set to 0.9 in this study. As a result, a total of τ strands are sampled from Γ_{inside} and stored in $\Gamma_{outside}$, representing the lost strands. The buffer that ultimately represents all the lost strands is $\Gamma_{outside}$.

3.4 | Changes in Back Volume Before and After Chemical Treatment

In this section, we propose a method for visualizing the back volume before and after chemical treatment in 3D. The key aspect of this process is to ensure that the increased volume at the back of the head is represented naturally. In this study, we use an anisotropic weighting function designed for long hairstyles to handle strand deformation and present a method for rapid visualization (see Figure 8).

For back volume, the change was measured using the horizontal length of the strands based on the gray boundary in the actual image (see Figure 1e). In reality, this length increases after chemical treatment. To visualize this change in 3D, this study uses Equation (10).

$$p^{strand}_i = p^{\oplus} + \nabla p \sigma_d W_A\left(p_i - p^{\oplus}, h\right) \tag{10}$$

$$W_A(\mathbf{r}, \mathbf{G}) = \sigma \|\mathbf{G}\| P(\|\mathbf{G}, \mathbf{r}\|) \tag{11}$$

where W_A is an anisotropic kernel, which differs significantly from the previously used kernels. Additionally, P is a symmetric decaying spline with finite support. In this study, an anisotropic kernel is utilized to compute the deformation weights corresponding to volume changes in long hair [47]. To achieve this, we first calculate the weighted average covariance of particle C as shown in Equation (12).

$$C_i = \frac{\sum_j \left(p_j - \bar{p}_i\right)\left(p_j - \bar{p}_i\right)^T W\left(p_j - \bar{p}_i, h\right)}{W\left(p_j - \bar{p}_i, h\right)} \tag{12}$$

where

$$\bar{p}_i = \frac{\sum_j p_j W\left(p_j - \bar{p}_i, h\right)}{W\left(p_j - \bar{p}_i, h\right)} \tag{13}$$

Using the Singular Value Decomposition (SVD) of the calculated C_i, the direction and stretch of the adjacent particles are determined based on eigenvectors and eigenvalues, as shown in Equation (14).

$$C_i = \mathbf{R}\Sigma\mathbf{R}^T = \begin{bmatrix} e^T_1 \\ e^T_2 \\ e^T_3 \end{bmatrix}^T \begin{bmatrix} \sigma_1 & & \\ & \sigma_2 & \\ & & \sigma_3 \end{bmatrix} \begin{bmatrix} e^T_1 \\ e^T_2 \\ e^T_3 \end{bmatrix} \tag{14}$$

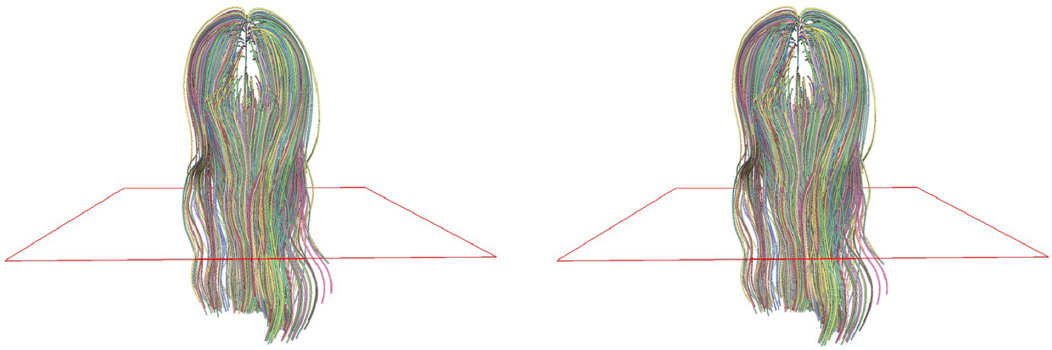

(a) Before : 21.6cm (b) After : 24.18cm

FIGURE 8 | Visualization of the back volume area before and after chemical treatment. The reference image for (a) is shown at the *left* of Figure 1e, while the reference image for (b) appears at the *right* of Figure 1e.

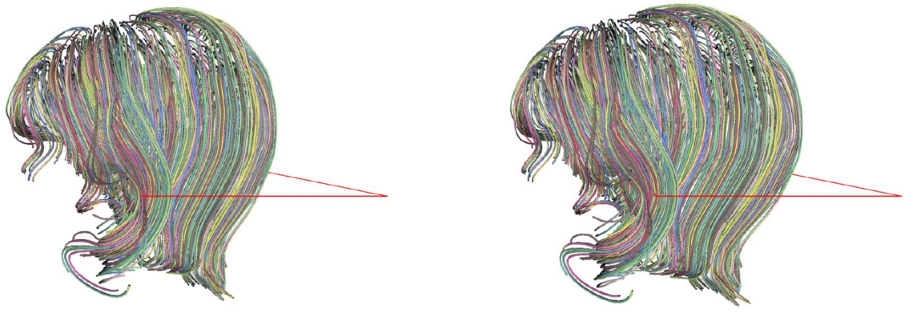

(a) Before : 25.89cm (b) After : 32.29cm

FIGURE 9 | *Visualization of the side volume area before and after chemical treatment.* The reference image for (a) is shown at the *left* of Figure 1d, while the reference image for (b) appears at the *right* of Figure 1d.

where e_n and σ_n represent the principal axes sorted according to variance and the degree of stretch, respectively. Then, Gi is computed in the form of a symmetric matrix (see Equation (15)).

$$\mathbf{G}_i = \frac{1}{h_i}\mathbf{R}\Sigma^{-1}\mathbf{R}^T \tag{15}$$

In Figure 8, the red line indicates the position aligned with the gray boundary in the actual image (see Figure 1e). The results demonstrate that hair deforms naturally according to the horizontal strand length at the boundary.

3.5 | Changes in Side Volume Before and After Chemical Treatment

In this section, we describe the method for visualizing the side volume before and after chemical treatment in 3D. Since this process requires natural expression of volume-based deformation by measuring the length change from behind the ear to the back of the head, experiments are conducted in short hairstyles where the area behind the ears is more visible. Similarly to back volume, strand deformation in this case also has directionality, so an anisotropic weighting function is used to efficiently process and visualize strand deformation (see Figure 9). In this scene, the deformation of the strand is applied using Equation (10), except for the reference position $p^{\oplus}$, which serves as the deformation anchor. In this study, $p^{\oplus}$ is set as follows: $\left(0.5, p_i^{strand}, 0.25\right)$.

4 | Implementation

This study was implemented in the following environment: Intel i7-7700k 4.20 GHz CPU, 32 GB RAM, NVIDIA GeForce GTX 1080 Ti graphics card.

Typically, thin shell materials are used to visualize hair and fur. However, since this study focuses on analysis rather than visual special effects (VFX), it prioritizes clearly representing strand volume and shape over realistic hair rendering techniques. Therefore, a cylindrical shape was generated from the strand lines to enhance the volumetric representation of the hair.

The proposed method visualizes 3D hair using measurements obtained from real hair. In this study, the volume changes were approximated based on the variation of length, as shown in Figure 10. Although this approach does not provide a perfectly

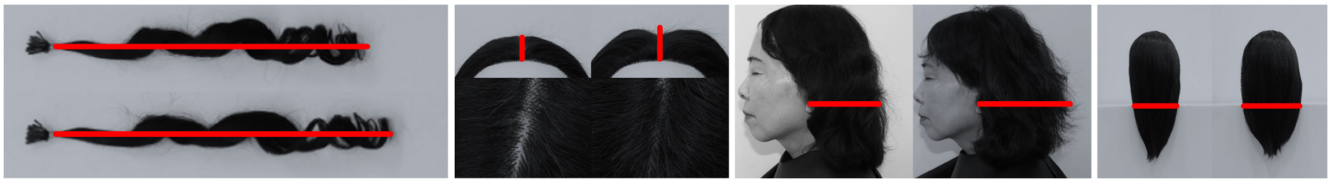

FIGURE 10 | Method for measuring changes in strand volume in real hair.

accurate representation of volume changes, it effectively highlights differences before and after chemical treatment. This limitation can be addressed in future work by using precise volume measurement devices.

5 | Experimental Results

In this section, we describe the composition of each scene and examine the 3D strand visualization results based on the previously conducted experiments. This study analyzes the changes in the hairs before and after chemical treatment in five different scenes (Figure 11).

Hair Sagging. In this experiment, a digital camera (Canon EOS 750D) and an image analysis program (ImageJ) were used to assess improvements in hair sagging. To ensure consistent photography, the position of both the hairpiece and the camera was fixed, maintaining a constant distance between the test area and the lens. All hairpieces were photographed with uniform lighting and identical positioning using a strobe light by the same test operator. The image analysis program was then used to measure the curvature changes in the captured hair images. An increase in the measured values compared to pre-treatment indicates an improvement in hair sagging.

Figure 12 visualizes hair sagging before and after chemical treatment using 3D strands. The key aspect of this scene is to clearly represent the sagging of hair, rather than focusing on the intensity of straight or curly hair forms. In this study, hair sagging is represented based on user-measured strand lengths, allowing for a more natural visualization by controlling the balance between straight and curly hair.

Hair Root Volume. To measure changes in root volume, the front area of all hair wigs was photographed. The captured images were analyzed using an image analysis program, measuring changes in hair height based on the center point of the wig. An increase in the measured values compared to pre-treatment indicates an improvement in hair root volume.

Figure 13 visualizes root volume before and after chemical treatment using 3D strands. The key aspect of this scene is the length from the center point to the top point (see Figure 11), which was used to approximate the changes in volume. In Figure 13a, representing the pre-treatment state, the area between the red planes shows a smaller volume, whereas in Figure 13b, after chemical treatment, a noticeable increase in volume can be observed.

Hair Crown Volume. To measure changes in crown volume, the top point of all hairpieces was photographed. The captured images were binarized using an image analysis program based on Otsu's thresholding method [48]. The binarized images were analyzed considering the white areas above the threshold as the visible scalp area, and the proportion of this area was evaluated relative to the total surface. A decrease in the measured values compared to pre-treatment indicates an improvement in hair crown volume.

Figure 14 visualizes crown volume before and after chemical treatment using 3D strands. In this scene, it is crucial to ensure a natural representation of the volume changes around the crown area before and after treatment. Figure 14a shows the 3D representation of the hair strands before treatment, while Figure 14b depicts a modified version with more severe hair loss. Figure 14c illustrates the post-treatment results, effectively representing the reduction in hair loss based on the measured values.

Hair Back Volume. To measure changes in hair back volume, the rear area of all hairpieces was photographed. Using the captured images, an image analysis program was used to analyze changes in hair width. The width of the hair was measured as the horizontal distance from the left ear point to the right ear point at the back of the hairpiece (see Figure 11). An increase in the measured values compared to pre-treatment indicates an improvement in hair back volume.

Figure 15 visualizes the back volume before and after chemical treatment using 3D strands. The measurement range for the back volume is represented by the red plane, and the changes in the back volume were assessed based on the horizontal length of the corresponding strands, which were then visualized in 3D. Figure 15a shows the pre-treatment results, while Figure 15b presents the post-treatment results. As shown in the figure, the changes in the back volume are effectively visualized based on the user-measured values.

Hair Side Volume. To measure changes in hair side volume, the temporal region of all test participants was photographed. The captured images were analyzed using an image analysis program to assess changes in hair width. The width of the hair was measured on the side ear point to assess variations in side volume (see Figure 11). An increase in the measured values compared to pre-treatment indicates an improvement in hair side volume.

Figure 16 visualizes hair side volume before and after chemical treatment using 3D strands. Similar to the previous results, the post-treatment visualization clearly demonstrates a more pronounced change in side volume compared to the pre-treatment state, effectively represented through the 3D strand model.

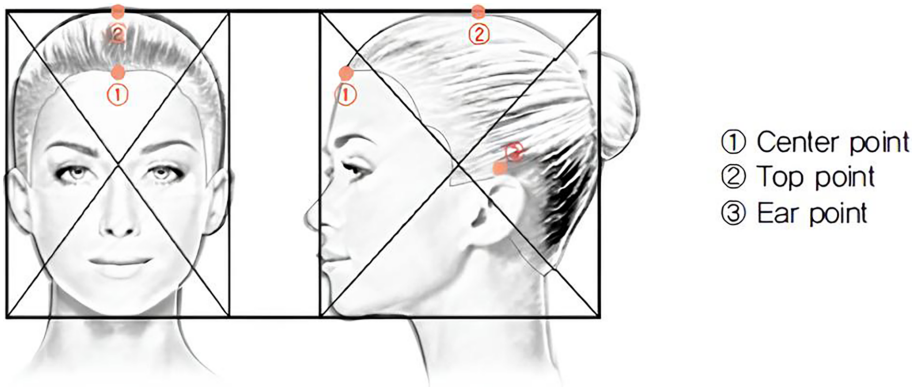

FIGURE 11 | Head points.

FIGURE 12 | Comparison of 3D strand changes in hair sagging (before: 24.4 cm, after: 15.0 cm).

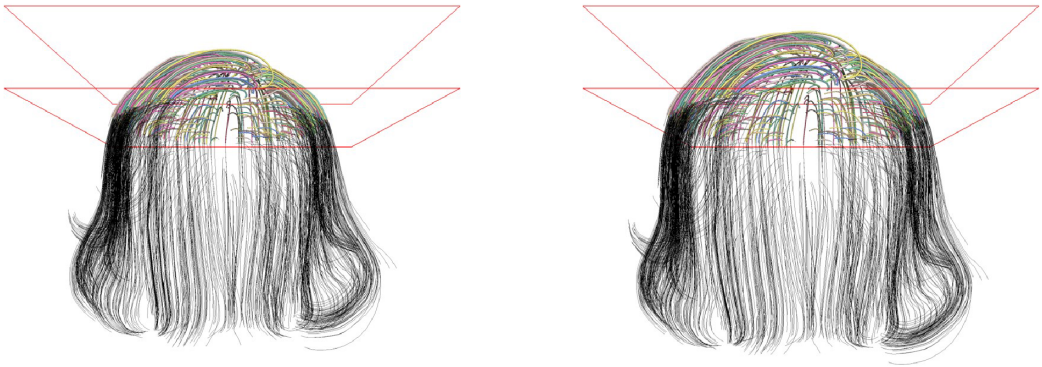

FIGURE 13 | Comparison of 3D strand changes in root volume.

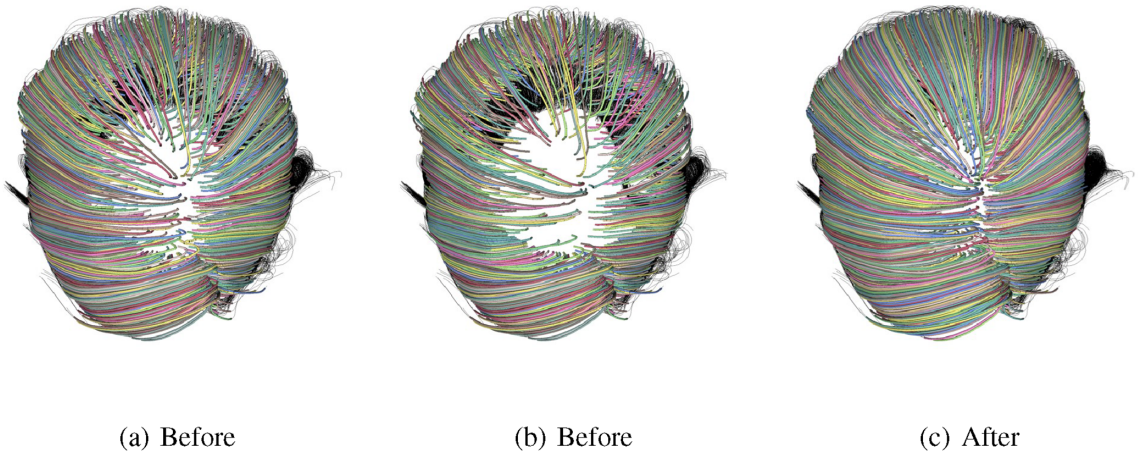

(a) Before (b) Before (c) After

FIGURE 14 | Comparison of 3D strand changes in crown volume.

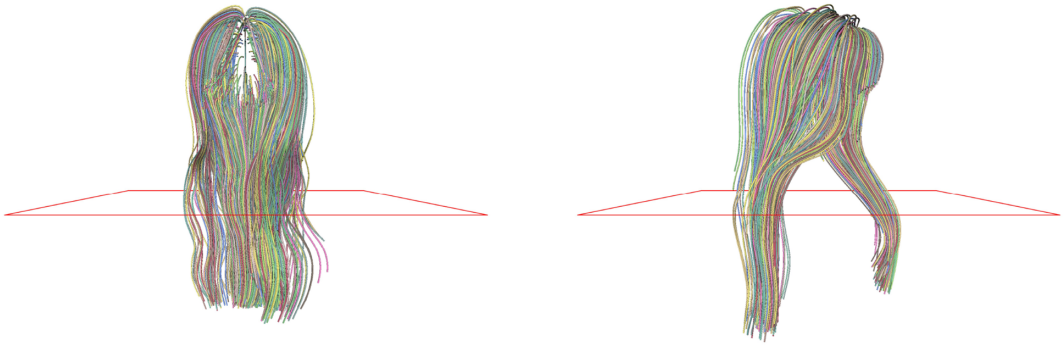

(a) Before : 21.6cm

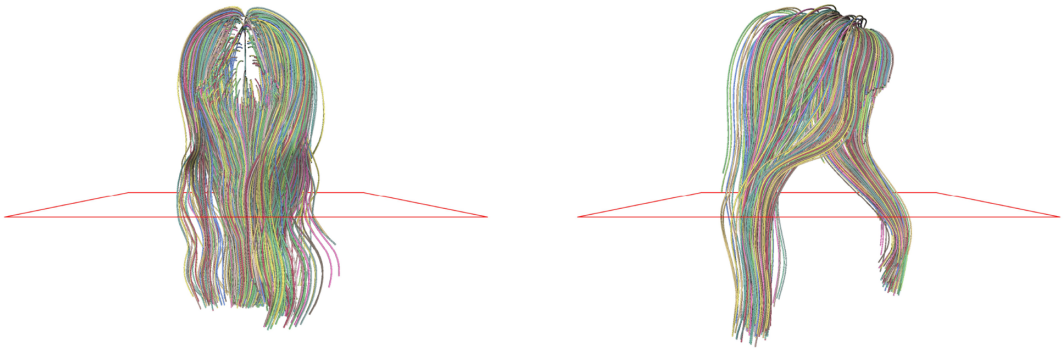

(b) After : 26.18cm

FIGURE 15 | Comparison of 3D strand changes in back volume.

6 | User Study Design

After a brief explanation of the proposed method, the application testers visualized and analyzed 3D strands in various scenes. They were then asked to complete a questionnaire (see Table 1) after using the proposed application. The primary objective was to assess how the application influenced the perception of volume changes before and after chemical treatment on 3D strands. To evaluate the proposed application, a survey was conducted with 24 researchers, aged 20 to 30, who study volume changes before and after chemical treatment.

Figure 17 presents the results of the survey conducted with 24 testers (Female: 21, Male: 3). Although most of the participants provided positive feedback, some expressed difficulties navigating the 3D view volume and observing the 3D strands. In general, the majority agreed that the 3D strand visualization effectively demonstrated changes in hair volume.

(a) Before : 25.89cm (b) After : 32.29cm

FIGURE 16 | Compare 3D strand results for side volume.

TABLE 1 | Questionnaire (Q1∼Q8: Satisfied (5), Normal (3), Not Satisfied (0)).

No.	Question description
Q1	After using this tool, were you able to easily understand the changes in hair volume before and after chemical treatment?
Q2	Was the visualization of this tool easy to use?
Q3	Did the visualization of this tool effectively show the changes in hair volume?
Q4	Did the visualization of this tool effectively show the differences before and after chemical treatment?
Q5	Did the visualization of this tool increase your confidence in the effects of the chemical treatment?
Q6	Would you be willing to use this tool again?
Q7	Would you be willing to recommend this tool to others?

7 | Discussion

This study aims to simulate changes in hair volume after chemical treatment using a 3D visualization tool. It is true, as you pointed out, that the chemical treatment itself—its type or ingredients—is not directly used as an input parameter in the model. Instead, we intentionally designed the system to focus solely on measuring and visualizing the changes in hair before and after treatment, regardless of the internal chemical processes involved. This approach simplifies the overall algorithm while still capturing the effects of treatment.

The following outlines how the proposed system operates within this framework.

System Operation:

1. Numerical inputs such as changes in length, volume, and position—measured through actual pre- and post-chemical treatment experiments—are provided to the system.
2. Based on these values, the system adjusts strand parameters—such as length ratio, curvature, and weight—for both straight and curly forms to generate the visualization.
3. In other words, the system does not simulate the chemical treatment itself, but rather visualizes the changes observed before and after the treatment.

In summary, the system quantitatively measures changes in hair length, volume, and curvature before and after chemical treatment using image analysis tools (e.g., ImageJ), and performs 3D visualization based on these measurements.

The heuristic parameters used in this study are not arbitrarily adjusted values, but rather ratios or weights derived from actual measured data. For example, values such as length change ratios, weights, and anisotropic kernels are set based on experimental data.

Real-World Applicability of the System

1. Product developers or researchers can visually analyze and compare the effects of cosmetic treatments.
2. Consumers can intuitively observe the effects of product use before and after treatment in 3D.
3. It can be used as compelling visual evidence in marketing or clinical trials.

Currently, the system does not automatically predict the results of chemical treatments, but it has strong potential as a tool for presenting experimental outcomes more intuitively through physics-based 3D visualization. In the future, it could be extended to incorporate chemical composition data for prediction or automation.

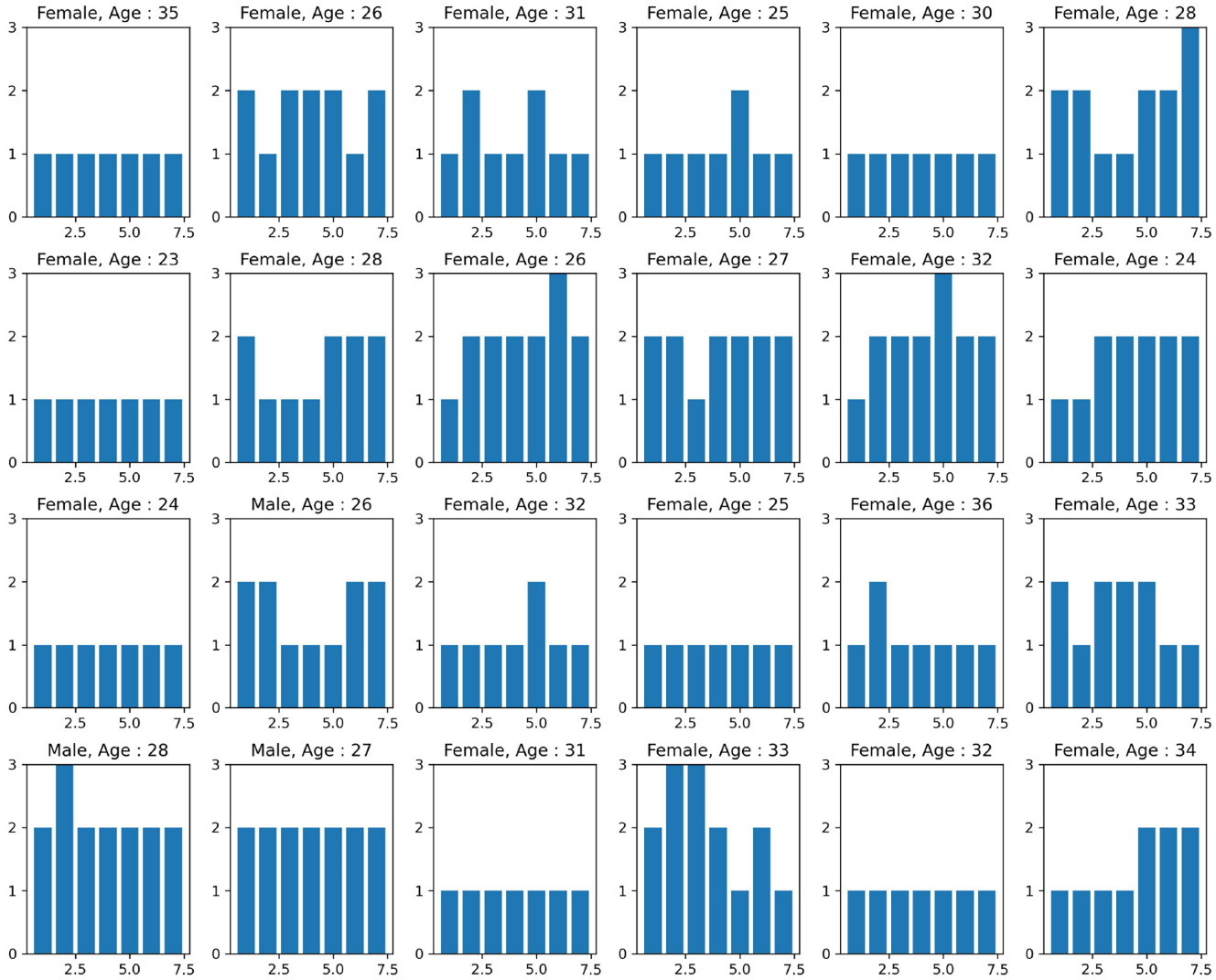

FIGURE 17 | Questionnaire result (*x*-axis: Number of question, *y*-axis: Score).

8 | Conclusion

In this study, we proposed a 3D visualization tool based on a physically-based simulation to effectively observe and analyze changes in hair volume and length after cosmetic and chemical treatments. Unlike virtual hair simulations, the proposed tool reflects the importance of real hair care by visually representing the effects of various chemical treatments on hair. The experimental results validated the effectiveness of the tool through performance evaluations in various scenarios, including back volume, root volume, side volume, crown volume, and hair sagging. This tool has the potential to be extended to skincare and other beauty-related fields, contributing to the evaluation of a wider range of cosmetics and chemical treatments. The findings of this study provide a new foundation for a scientific approach in the beauty industry and are expected to make a meaningful contribution to related industries.

Conflicts of Interest

The authors declare no conflicts of interest.

Data Availability Statement

The data that support the findings of this study are available from the corresponding author upon reasonable request.

References

1. K. Ward, F. Bertails, T.-Y. Kim, S. R. Marschner, M.-P. Cani, and M. C. Lin, "A Survey on Hair Modeling: Styling, Simulation, and Rendering," *IEEE Transactions on Visualization and Computer Graphics* 13, no. 2 (2007): 213–234.

2. A. Daldegan, N. Magnenat Thalmann, T. Kurihara, and D. Thalmann, "An Integrated System for Modeling, Animating and Rendering Hair," *Computer Graphics Forum* 12 (1993): 211–221. Wiley Online Library.

3. Y. Bao and Y. Qi, "A Survey of Image-Based Techniques for Hair Modeling," *IEEE Access* 6 (2018): 18670–18684.

4. M. Feughelman, "Physical Properties of Hair," in *Hair and Hair Care* (Routledge, 2018), 13–32.

5. T. Mieczkowski, A. M. Tsatsakis, M. Kruger, and T. Psillakis, "The Concentration of Three Anti-Seizure Medications in Hair: The Effects of Hair Color, Controlling for Dose and Age," *BMC Clinical Pharmacology* 1 (2001): 1–12.

6. S. Paris, H. M. Briceno, and F. X. Sillion, "Capture of Hair Geometry From Multiple Images," *ACM Transactions on Graphics (TOG)* 23, no. 3 (2004): 712–719.

7. Y. Wei, E. Ofek, L. Quan, and H.-Y. Shum, "Modeling Hair From Multiple Views," in *ACM SIGGRAPH 2005 Papers* (ACM, 2005), 816–820.

8. S. Paris, W. Chang, O. I. Kozhushnyan, et al., "Hair Photobooth: Geometric and Photometric Acquisition of Real Hairstyles," *ACM Transactions on Graphics* 27, no. 3 (2008): 30.

9. W. Jakob, J. T. Moon, and S. Marschner, "Capturing Hair Assemblies Fiber by Fiber," in *ACM SIGGRAPH Asia 2009 Papers* (ACM, 2009), 1–9.

10. M. Chai, L. Wang, Y. Weng, Y. Yizhou, B. Guo, and K. Zhou, "Single-View Hair Modeling for Portrait Manipulation," *ACM Transactions on Graphics (TOG)* 31, no. 4 (2012): 1–8.

11. M. Chai, L. Wang, Y. Weng, X. Jin, and K. Zhou, "Dynamic Hair Manipulation in Images and Videos," *ACM Transactions on Graphics (TOG)* 32, no. 4 (2013): 1–8.

12. T. Beeler, B. Bickel, G. Noris, et al., "Coupled 3d Reconstruction of Sparse Facial Hair and Skin," *ACM Transactions on Graphics* 31, no. 4 (2012): 1–10.

13. T. L. Herrera, A. Zinke, and A. Weber, "Lighting Hair From the Inside: A Thermal Approach to Hair Reconstruction," *ACM Transactions on Graphics (TOG)* 31, no. 6 (2012): 1–9.

14. L. Luo, H. Li, S. Paris, T. Weise, M. Pauly, and S. Rusinkiewicz, "Multi-View Hair Capture Using Orientation Fields," in *2012 IEEE Conference on Computer Vision and Pattern Recognition* (IEEE, 2012), 1490–1497.

15. L. Luo, C. Zhang, Z. Zhang, and S. Rusinkiewicz, "Wide-Baseline Hair Capture Using Strand-Based Refinement," in *Proceedings of the IEEE Conference on Computer Vision and Pattern Recognition* (IEEE Computer Society, 2013), 265–272.

16. L. Luo, H. Li, and S. Rusinkiewicz, "Structure-Aware Hair Capture," *ACM Transactions on Graphics (TOG)* 32, no. 4 (2013): 1–12.

17. H. Liwen, C. Ma, L. Luo, and H. Li, "Robust Hair Capture Using Simulated Examples," *ACM Transactions on Graphics (TOG)* 33, no. 4 (2014): 1–10.

18. L. Hu, C. Ma, L. Luo, and H. Li, "Single-View Hair Modeling Using a Hairstyle Database," *ACM Transactions on Graphics* 34, no. 4 (2015): 1–9.

19. M. Chai, L. Luo, K. Sunkavalli, N. Carr, S. Hadap, and K. Zhou, "High-Quality Hair Modeling From a Single Portrait Photo," *ACM Transactions on Graphics* 34, no. 6 (2015): 201–204.

20. M. Chai, T. Shao, H. Wu, Y. Weng, and K. Zhou, "Autohair: Fully Automatic Hair Modeling From a Single Image," *ACM Transactions on Graphics* 35, no. 4 (2016): 1–12.

21. M. Zhang, M. Chai, H. Wu, H. Yang, and K. Zhou, "A Data-Driven Approach to Four-View Image-Based Hair Modeling," *ACM Transactions on Graphics* 36, no. 4 (2017): 151–156.

22. V. Sklyarova, J. Chelishev, A. Dogaru, I. Medvedev, V. Lempitsky, and E. Zakharov, "Neural Haircut: Prior-Guided Strand-Based Hair Reconstruction," in *2023 IEEE/CVF International Conference on Computer Vision (ICCV)* (ACM, 2023), 19762–19773.

23. K. Wu, L. Yang, Z. Kuang, et al., "Monohair: High-Fidelity Hair Modeling From a Monocular Video," in *Proceedings of the IEEE/CVF Conference on Computer Vision and Pattern Recognition* (IEEE, 2024), 24164–24173.

24. Y. Zhou, M. Chai, D. Wang, et al., "Groomcap: High-Fidelity Prior-Free Hair Capture," *ACM Transactions on Graphics (TOG)* 43, no. 6 (2024): 1–15.

25. M. Müller, B. Heidelberger, M. Hennix, and J. Ratcliff, "Position Based Dynamics," *Journal of Visual Communication and Image Representation* 18, no. 2 (2007): 109–118.

26. J. Bender, M. Müller, M. A. Otaduy, and M. Teschner, "Position-Based Methods for the Simulation of Solid Objects in Computer Graphics," in *EUROGRAPHICS 2013 State of the Art Reports* (The Eurographics Association, 2013), 1–22.

27. M. Miles and M. Matthias, "Position Based Fluids," *ACM Transactions on Graphics* 32, no. 4 (2013): 1–12.

28. M. Macklin, M. Müller, N. Chentanez, and T.-Y. Kim, "Unified Particle Physics for Real-Time Applications," *ACM Transactions on Graphics* 33, no. 4 (2014): 1–12.

29. M. Müller, T.-Y. Kim, and N. Chentanez, "Fast Simulation of Inextensible Hair and Fur," *Vriphys* 12 (2012): 39–44.

30. D. Han and T. Harada, "Real-Time Hair Simulation With Efficient Hair Style Preservation," 2012.

31. T.-Y. Kim, N. Chentanez, and M. Müller-Fischer, "Long Range Attachments-A Method to Simulate Inextensible Clothing in Computer Games," in *Proceedings of the ACM SIGGRAPH/Eurographics Symposium on Computer Animation* (The Eurographics Association, 2012), 305–310.

32. N. Umetani, R. Schmidt, and J. Stam, "Position-Based Elastic Rods," in *ACM SIGGRAPH 2014 Talks* (The Eurographics Association, 2014), 1.

33. S. Hadap and N. Magnenat-Thalmann, "Modeling Dynamic Hair as a Continuum," *Computer Graphics Forum* 20 (2001): 329–338.

34. A. Selle, M. Lentine, and R. Fedkiw, "A Mass Spring Model for Hair Simulation," in *ACM SIGGRAPH 2008 Papers* (ACM, 2008), 1–11.

35. M. Bergou, M. Wardetzky, S. Robinson, B. Audoly, and E. Grinspun, "Discrete Elastic Rods," in *ACM SIGGRAPH 2008 Papers* (ACM, 2008), 1–12.

36. F. Bertails, B. Audoly, M.-P. Cani, B. Querleux, F. Leroy, and J.-L. Lévêque, "Super-Helices for Predicting the Dynamics of Natural Hair," *ACM Transactions on Graphics* 25, no. 3 (2006): 1180–1187.

37. M. Atzmon, N. Haim, L. Yariv, O. Israelov, H. Maron, and Y. Lipman, "Controlling Neural Level Sets," in *Advances in Neural Information Processing Systems*, vol. 32 (NeurIPS Foundation, 2019).

38. M. Michalkiewicz, J. K. Pontes, D. Jack, M. Baktashmotlagh, and A. Eriksson, "Implicit Surface Representations as Layers in Neural Networks," in *2019 IEEE/CVF International Conference on Computer Vision (ICCV)* (IEEE/CVF, 2019), 4743–4752.

39. J. J. Park, P. Florence, J. Straub, R. Newcombe, and S. Lovegrove, "Deepsdf: Learning Continuous Signed Distance Functions for Shape Representation," in *Proceedings of the IEEE/CVF Conference on Computer Vision and Pattern Recognition* (IEEE/CVF, 2019), 165–174.

40. S. Peng, M. Niemeyer, L. Mescheder, M. Pollefeys, and A. Geiger, "Convolutional Occupancy Networks," in *Computer Vision–ECCV 2020: 16th European Conference, Glasgow, UK, August 23–28, 2020, Proceedings, Part III 16* (Springer, 2020), 523–540.

41. L. Mescheder, M. Oechsle, M. Niemeyer, S. Nowozin, and A. Geiger, "Occupancy Networks: Learning 3d Reconstruction in Function Space," in *Proceedings of the IEEE/CVF Conference on Computer Vision and Pattern Recognition* (IEEE/CVF, 2019), 4460–4470.

42. M. Denninger and R. Triebel, "3d Scene Reconstruction From a Single Viewport," in *European Conference on Computer Vision* (Springer, 2020), 51–67.

43. Z. Murez, T. Van As, J. Bartolozzi, A. Sinha, V. Badrinarayanan, and A. Rabinovich, "Atlas: End-To-End 3d Scene Reconstruction From Posed Images," in *Computer Vision–ECCV 2020: 16th European Conference, Glasgow, UK, August 23–28, 2020, Proceedings, Part VII 16* (Springer, 2020), 414–431.

44. S. Peng, Y. Zhang, Y. Xu, et al., "Neural Body: Implicit Neural Representations With Structured Latent Codes for Novel View Synthesis of Dynamic Humans," in *Proceedings of the IEEE/CVF Conference on Computer Vision and Pattern Recognition* (IEEE/CVF, 2021), 9054–9063.

45. S. Saito, Z. Huang, R. Natsume, S. Morishima, A. Kanazawa, and H. Li, "PIFu: Pixel-Aligned Implicit Function for High-Resolution Clothed Human Digitization," in *2019 IEEE/CVF International Conference on Computer Vision (ICCV)* (IEEE/CVF, 2019), 2304–2314.

46. C. Jiang, A. Sud, A. Makadia, et al., "Local Implicit Grid Representations for 3d Scenes," in *Proceedings of the IEEE/CVF Conference on Computer Vision and Pattern Recognition* (IEEE/CVF, 2020), 6001–6010.

47. Y. Jihun and G. Turk, "Reconstructing Surfaces of Particle-Based Fluids Using Anisotropic Kernels," *ACM Transactions on Graphics (TOG)* 32, no. 1 (2013): 1–12.

48. N. Otsu, "A Threshold Selection Method From Gray-Level Histograms," *Automatica* 11, no. 285-296 (1975): 23–27.